Journal of Agricultural Engineering

Journal of Agricultural Engineering 2026; LVII:1971
doi:10.4081/jae.2026.1971

Analysis of temperature distribution in a naturally ventilated single-span greenhouse using computational fluid dynamics

Oluwasegun Moses Ogundele,[1] Jung-Hoo Kook,[2] Sang-Min Kim,[2] Jeong-In Choi,[2] Niraj Tamrakar,[1] Sijan Karki,[1] Reginald Gbenga Azuatalam,[1] Timothy Denen Akpenpuun,[3] Hyeon Tae Kim[1]

[1]Department of Bio-systems Engineering, Gyeongsang National University, Institute of Smart Space Agriculture (ISSA), Jinju, Korea; [2]Department of Smart Farm, Gyeongsang National University, Institute of Smart Space Agriculture (ISSA), Jinju, Korea; [3]Department of Agricultural and Biosystems Engineering, University of Ilorin, Nigeria

Abstract

Increasing global temperatures and unpredictable weather threaten agricultural production, intensifying the reliance on greenhouse cultivation. While naturally ventilated greenhouses offer an energy-efficient solution, their thermal performance under high heat loads is a growing concern. This study developed and validated a 3D CFD model to investigate the temperature distribution inside a single-span, naturally ventilated greenhouse. The model, implemented in ANSYS Fluent, considered the influence of external meteorological conditions, including solar radiation and wind, on the internal microclimate. The model demonstrated high accuracy, with a root mean square error of 0.847°C and a mean absolute error of 0.714°C for temperature when compared to experimental data. Diurnal analysis confirmed the dominant role of solar radiation, showing a strong correlation between indoor temperature and external solar radiation (r=0.96) on sunny days. Spatially, the simulation revealed extreme thermal heterogeneity under high solar load, with a total internal temperature variation of up to 25°C (from 296 K to 321 K). The distribution was characterized by a distinct vertical stratification due to buoyancy and a strong longitudinal gradient, with the hottest air accumulating in the upper leeward corner. These findings highlight areas of potential crop heat stress and demonstrate the limitations of side-ventilation alone. The validated model serves as a valuable tool for optimizing ventilation strategies and improving climate control system design.

Key words: CFD model; greenhouse; temperature distribution; ventilation optimization.

Correspondence: Hyeon Tae Kim, Department of Bio-systems Engineering, Gyeongsang National University, Institute of Smart Space Agriculture (ISSA), Jinju 52828, Republic of Korea. E-mail: bioani@gnu.ac.kr

Introduction

In recent decades, anthropogenic activities have exacerbated changes in the Earth's atmospheric conditions, resulting in rising global temperatures, water scarcity, and increasingly unpredictable weather patterns (Gołasa *et al*., 2021; Khudoyberdiev *et al*., 2021). These environmental changes have negatively impacted agricultural production, which is already under pressure to meet the demands of a growing global population projected to reach 9.8 billion by 2050 (Elanchezhian *et al*., 2020; Revathi *et al*., 2021). To mitigate these challenges, the adoption of crop protection techniques, commonly called "protected agriculture", has been gaining global attention due to its potential to address food security concerns (Lawrence *et al*., 2017; Amara *et al*., 2021; Blanco *et al*., 2022). These methods allow for the cultivation of crops within enclosed structures where microclimatic conditions critical for crop growth and development are either fully or partially controlled (Lamichhane *et al*., 2023). Among these methods, greenhouse cultivation is the most dominant and has been widely deployed to support the increasing population. Compared with conventional open-field agriculture, greenhouses create a more favorable environment for crop growth by regulating the indoor climate (Li *et al*., 2025). This controlled setting shields crops from unfavorable outdoor weather conditions and other external aggressors such as insects, pests, and diseases (Ghani *et al*., 2020), increases yield per unit of available land area, improves quality of crops (Choab *et al*., 2019), improves irrigation management and controlled inputs (Villagran *et al*., 2021), extends growing periods, and off-season crop production (Akpenpuun *et al*., 2023a).

The overall greenhouse microclimate is significantly impacted by several environmental factors, but among these, temperature is arguably the most critical, directly affecting photosynthesis, respiration, and plant stress (Hou *et al*., 2021). Therefore, precise control of thermal conditions is paramount to facilitate proper management strategies and growing conditions for crops. Comparatively speaking, although recent developments in greenhouse facilities through the integration of automated systems have enhanced control over the greenhouse microclimate, this level of control comes at a considerable cost, both in terms of installation and operational expenses. As a result, many regions in Asia and countries on the Mediterranean coast, where natural ventilation is effective not only in the summer but also during other periods pf the year, , widely use passive greenhouses that utilize natural ven-

tilation to regulate the internal climate as a cost-effective alternative (Villagran *et al*., 2021). These greenhouses operate on the principle of air exchange between the internal and external environment through vents and openings, which supports the passive ventilation process. This process removes heat trapped from solar radiation and expels water vapor from evapotranspiration. Since natural wind energy, a renewable resource, powers this mechanism, it consumes minimal energy and qualifies as an environmentally sustainable option (Villagrán *et al*., 2019; Akpenpuun *et al*., 2023b).

Despite the merits of natural ventilation, its effectiveness is considerably impacted by the often nonlinear and stochastic nature of outdoor weather conditions. With rising global temperatures, the feasibility of relying solely on natural ventilation to prevent heat stress during peak summer months is becoming increasingly difficult. This dependence on climate stability poses a challenge in maintaining a stable indoor climate, which is essential for optimal plant growth and development. In addition to the external environmental factors, the efficiency of a naturally ventilated system is also dependent on various design parameters such as greenhouse roof geometry, number of spans, vent configuration (mainly side vents, roof vents, or a combination of both), size, and positioning of greenhouse vents (Villagrán *et al*., 2019; Yin *et al*., 2024). Consequently, careful consideration of these design factors alongside a comprehensive understanding of the complex temperature distribution within the greenhouse is required when designing new systems

In earlier studies conducted on the natural ventilation of greenhouses, researchers have employed different approaches utilizing field analysis, such as tracer gas techniques, energy balance studies, scale methods, and direct and indirect experimentation (Villagrán *et al*., 2019; Akrami *et al*., 2020b). However, these methods are prone to several constraints that limit their consistent implementation, including difficulty in controlling variables due to unstable and unpredictable weather, reliance on a limited number of instruments for point measurement, and significant issues related to cost, labor, and time consumption (Kim *et al*., 2017; Lee *et al*., 2018). Recently, researchers in agriculture have turned their attention to computational fluid dynamics (CFD) to investigate natural ventilation in greenhouses (Ayuga, 2015; Chu *et al*., 2017).

CFD is a powerful and cost-effective tool that allows for detailed analysis of complex airflow and thermal patterns. It employs numerical methods to solve the non-linear equations that govern fluid flow and heat transfer. The built-in advantages of CFD software include rapid prediction speeds and the ability to simulate a wide array of unbuilt scenarios, making it an essential tool for comprehending and optimizing thermal dynamics in naturally ventilated greenhouses. In recent years, CFD methods have been widely employed to study the effects of the different design factors and environmental conditions affecting naturally ventilated greenhouses. For instance, the ventilation performance of a Chinese solar greenhouse was evaluated by Zhang *et al*. (2022) by proposing a novel front bottom + top + back roof (FTB) configuration. They found that the FTB configuration reduced the time needed to stabilize the greenhouse temperature and improve the cooling rate, improving ventilation efficiency and uniformity. In addition, Benni *et al*. (2016) explored optimal vent configurations and management procedures for summer cooling in an Italian greenhouse using CFD simulation. The study compared various roof vent scenarios, with side wall vents consistently open, and found that closing the windward roof vent achieved 64% of maximum heat removal, outperforming other configurations that reached around 50%. Villagrán *et al*. (2019) utilized a transient CFD- Two Dimensional (2D) model to analyze natural ventilation in three types of greenhouses: a traditional Colombian wood (TG) greenhouse and two alternative multi-span greenhouses, curved (DMG) and gothic (GMG), characterized by larger side and roof ventilation areas. The simulations demonstrated that both DMG and GMG achieved ventilation rates 3.4 times higher than TG, leading to a more homogeneous thermal distribution and reducing average temperatures by 2.8°C compared to TG.

Although previous studies have utilized CFD to study naturally ventilated greenhouses by varying different design and environmental factors to optimize the greenhouse microclimate and have established a solid scientific foundation for CFD studies of natural ventilation dynamics in plant production systems, the literature review found that the majority have focused on the internal environment while excluding the influence of the outdoor environment, and the effect of radiation on greenhouse conditions. Therefore, this research aims to analyze the temperature distribution within the greenhouse environment through the use of an external computational domain and the discrete ordinate (DO) radiation model for radiation effect for a detailed thermal analysis. Hence, a 3D CFD model was developed and experimentally validated through field measurements in a single-span greenhouse located in South Korea.

Materials and Methods

Study area

Field measurements required to design and validate the CFD model were collected at an experimental greenhouse managed by the Smart Space Sensing Laboratory (SSSL) at Gyeongsang National University, located in Jinju, Gyeongsangnam-do (South Gyeongsang Province), South Korea, at latitude N35.09° and longitude 128.05°. Jinju, Gyeongsangnam-do has a humid subtropical climate characterized by four distinct seasons: Spring (March to May), Summer (June to August), Fall (September to November), and Winter (December to February), with an annual average temperature, precipitation, relative humidity, and wind speed of 13.4°C, 1518 mm, 67.5% and 1.4 m/s respectively (Korean Meteorological Administration). The region is known for its agricultural production, including rice, barley, strawberries, persimmons, watermelons, and various vegetables.

Experimental setup and data collection

The experimental greenhouse had a flat, arch-shaped structure oriented East-West (E-W) and was covered with two layers of ultraviolet (UV) resistant polyethylene of 0.1 mm and 0.075 mm. The greenhouse dimensions were 19.7 m × 7.7 m × 3.6 m, providing a total floor area of 136.29 m^2. It was naturally ventilated with two roll-up side vents located 1.5 m above the ground with a maximum area of 1 m^2.

Two heating fans, typically used during the winter period, were installed at the eastern and western ends of the greenhouse along the central axis at a height of 1.75 m. However, these fans remained inactive throughout the summer experimental period, as the study focused on evaluating the effects of natural ventilation without the influence of forced ventilation.

The greenhouse under test consisted of five raised cultivation beds, each characterized by a height of 1.5 m and a width of 0.75 m; each bed is spaced 0.5 m apart to align with the greenhouse structure and maximize solar radiation exposure. The variables

inside the greenhouse were air temperature, relative humidity, and solar radiation, while the external variables were temperature, relative humidity, solar radiation, and wind speed and direction. During the experimental period, no crops were cultivated in the greenhouse. Indoor temperature and relative humidity were measured using HOBO PRO v2 U23 Pro v2 sensors (Onset Computer Co., Bourne, MA, USA; temperature measurement range -20°C to 80°C, accuracy of ±0.25°C; humidity measurement range of 0% to 100%, accuracy of ±2%). These sensors were located at the front, center, and rear of the greenhouse at locations corresponding to where crop rows would typically be placed, all positioned at a height of 1 m from the ground level. The solar radiation sensors (HOBO RX3000, Onset Computer Co.; measurement range: 0 to 1280 W/m^2; accuracy: ±10 W/m^2, operating temperature range: -40°C to 70°C) were placed at the same locations as the temperature and humidity sensors. Outdoor weather data, including temperature, relative humidity, wind speed and direction, and solar radiation, was collected from an outdoor weather station. Figure 1 shows a schematic diagram of the experimental greenhouse, and a layout of the experimental greenhouse showing the sensor locations.

Computational fluid dynamics

The airflow and thermal behavior inside the greenhouse were simulated using CFD. The model solves the governing equations for mass, momentum, and energy conservation, which describe the coupled airflow and heat transfer processes under transient conditions. These equations are well established in fluid dynamics and have been widely applied in greenhouse ventilation studies. All mathematical formulations of the continuity, momentum, and energy equations, including all variables, are provided in the Supplementary Material.

Turbulence model

The k- turbulence model is one of the most common turbulence models used in CFD for simulating turbulent airflow due to its robustness, computational efficiency, and reasonable accuracy. One of the fundamental assumptions in the derivation of the k- model is that the flow is fully turbulent, allowing the effects of kinematic viscosity to be neglected. This assumption holds for the atmospheric boundary layer, where airflow is dominated by turbulence. Similarly, in greenhouses, the internal airflow is significantly influenced by structural geometry, which impedes flow patterns and induces turbulent fluctuations.

Several researchers have utilized CFD to simulate the microclimate inside greenhouses, applying different turbulence models to assess accuracy and computational cost. For instance, Nebbali *et al*. (2006) and Santolini *et al*. (2018) performed comparative studies on various turbulence models, including the Standard k- RNG k-, and Realizable k- models. Their findings indicate that the Standard k- model provided the most accurate predictions of greenhouse airflow dynamics while maintaining a lower computational cost compared to more complex models. Hence, in this study, the standard k- model is used as a result of its proven accuracy in predicting turbulent airflow in similar environments.

$$\frac{\partial}{\partial t}(\rho k) + \frac{\partial}{\partial x_i}(\rho k u_i) = \frac{\partial}{\partial x_j}\left[\left(\mu + \frac{\mu_t}{\sigma_k}\right)\frac{\partial k}{\partial x_j}\right] + G_k + G_b - \rho\varepsilon - Y_M + S_k \quad \text{(Eq. 1)}$$

$$\frac{\partial}{\partial t}(\rho\varepsilon) + \frac{\partial}{\partial x_i}(\rho\varepsilon u_i) = \frac{\partial}{\partial x_j}\left[\left(\mu + \frac{\mu_t}{\sigma_\varepsilon}\right)\frac{\partial \varepsilon}{\partial x_j}\right] + C_{1\varepsilon}\frac{\varepsilon}{k}(G_k + C_{3\varepsilon}G_b) - C_{2\varepsilon}\rho\frac{\varepsilon^2}{k} + S_\varepsilon \quad \text{(Eq. 2)}$$

where ρ represents the fluid density, while denotes the turbulent kinetic energy. The variable t corresponds to time. The quantities u_i and u_j signify the instantaneous velocity components in the directions of x_i and x_j, respectively. The term μ denotes the laminar dynamic viscosity, whereas the turbulent dynamic viscosity μ_t is given by $u_t = \rho C_u (k^2/\varepsilon)$, where C_μ is an empirical coefficient with a typical value of 0.085. The variable ε represents the turbulent dissipation rate. G_k accounts for the generation of turbulent kinetic energy due to velocity gradients, while G_b represents the production of k resulting from buoyancy effects. The parameter captures Y_M the influence of compressibility-induced turbulence fluctuations on the overall dissipation rate. The source term S_K is a user-defined parameter. The factors σ_k and σ_e correspond to the inverse effective turbulent Prandtl number for k and ε, respectively. According to established references, the constants typically take the values $\sigma_k = 1.0$, $\sigma_e = 1.3$, $C_{1\varepsilon} = 1.44$, and $C_{2\varepsilon} = 1.92$ (Senhaji *et al*., 2019; Akrami *et al*., 2020a).

Radiation model

The DO model was used to describe the coupled convective and radiative exchange occurring on the roof and walls of the greenhouse. The DO model has proven to be useful in modeling structures with opaque, transparent, and optical materials such as glass, plastic, air, thin films, and soil, and has been used in similar studies involving greenhouse CFD simulations (Ghani *et al*., 2020; Bazgaou *et al*., 2023; Yin *et al*., 2024):

$$\nabla(I(\vec{r},\vec{s})\vec{s} + (a+\sigma_s)I(\vec{r},\vec{s})) = an^2\frac{\sigma T^4}{\pi} + \frac{\sigma_s}{4\pi}\int_0^{4\pi} I(\vec{r},\vec{s})\emptyset(\vec{s},\vec{s})d\Omega' \quad \text{(Eq. 3)}$$

where $\vec{r}$ is the position vector, $\vec{s}$ is the direction vector, S is the scattering direction, s is the length along the route, a is the absorption coefficient, σ is the Stefan-Boltzmann constant, σ_s is the dispersion coefficient, I is the radiation intensity, which depends on position $\vec{r}$ and direction $\vec{s}$, T is the local temperature, ∇ is the divergence operator, $\emptyset$ is the phase function and Ω is the solid angle of radiation.

Numerical procedure

In this study, CFD simulations were conducted using a commercial software, ANSYS Workbench 2023 (ANSYS Inc., Canonsburg, PA, USA), on a desktop computer equipped with an Intel® Core™ i7 processor and 16GB RAM. The 3D greenhouse geometry was created using ANSYS Design Modeler. The geometry was configured to match the dimensions of the experimental greenhouse as discussed in previous section, with the x-axis oriented east, the y-axis directed upward, and the z-axis aligned south. The experimental greenhouse was covered with two layers of polyethylene films of 0.10 mm and 0.075 mm and was represented in the CFD model as a single polyethylene layer with 0.175mm to preserve the overall thermal resistance and radiative behavior of multi-layer films and avoiding excessive meshing at the roof interface.

The interaction between the greenhouse and its external environment was a critical aspect of the investigation, as it significantly influences the internal microclimate. To enhance computational efficiency and accuracy, the dimensions of the computational domain were defined relative to the maximum height of the structure (H = 3.6 m), following established best practices and guidelines (Lee *et al*., 2018). Figure 2 illustrates the computational domain, with distances of 3H, 15H, and 5H from the rooftop representing the upstream, downstream, and upper extents of the greenhouse.

The meshing process was performed using ANSYS meshing. This process involved dividing the greenhouse geometry and computational domain into smaller, discretized units. An unstructured tetrahedral mesh was utilized with 1001096 nodes and 5795811 elements. Mesh refinement was applied around the side vents to ensure accuracy. The mesh structure is illustrated in Figure 3.

The quality of the mesh was evaluated through the skewness (<0.95) and orthogonal quality (close to 1) to ensure reliable simulation results. These metrics help predict potential convergence issues and ensure numerical stability, and have been widely recognized in the literature for their utility (Zhang *et al*., 2019; Yeo *et al*., 2022).

The boundary conditions within the limits of the computational domain were established, with the left and right side boundaries defined as the airflow inlet and pressure outlet, respectively. The upper and lower boundaries of the computational domain, the greenhouse walls, roof, and floor are set as wall boundaries, and the vent areas are set as inlet and outlet boundaries. The physical and optical properties and boundary conditions are described in Tables 1 and 2 (Li *et al*., 2022; Senhaji *et al*., 2019) .

The airflow within the greenhouse was modeled as turbulent using the standard K-epsilon model as previously discussed. The Semi-Implicit Method for Pressure-Linked Equations (SIMPLE) was employed for pressure-velocity coupling, and the Second-Order Upwind scheme was used for discretization. To ensure solution accuracy, convergence criteria were set to 10^{-6} for the energy equation and 10^{-3} for other variables. Additionally, as discussed, the DO radiation model was activated to simulate the effects of solar and atmospheric radiation on heat transfer and temperature distribution.

Since the experiment was conducted in an empty greenhouse, the effects of crop transpiration, which primarily influences humidity, were not considered. This approach aligns with several studies that analyze greenhouse environments under critical, empty conditions to provide results applicable to various crop types (Aguilar-Rodríguez *et al*., 2021; Yin *et al*., 2024).

Table 1. Physical and optical properties used for simulation.

Property	Air	Polyethylene	Ground
Density (kg/m^3)	1.225	923	2100
Specific heat (J/kg/K)	1006.43	2300	880
Thermal conductivity (W/m/K)	0.0242	0.38	1.4
Absorption coefficient	0.19	0.37	0.6
Scattering coefficient	0.00	0.30	1
Refractive index	1.00	1.92	1
Emissivity	0.86	0.80	0.71

Table 2. Boundary conditions used for the simulation.

Parameter	Value
Airflow inlet	Velocity entrance (wind speed)
Pressure outlet	Pressure outlet (Atmospheric pressure: 101,325 pa)
Acceleration due to gravity	9.81m/s^2
Coefficient of viscosity	1.7894×10^{-5}
Turbulence model	Standard K-epsilon model
Pressure-velocity coupling	SIMPLE algorithm
Discretization scheme	Second-Order Upwind
Convergence criteria	1×10^{-6} (energy) and 1×10^{-3} (other variables)

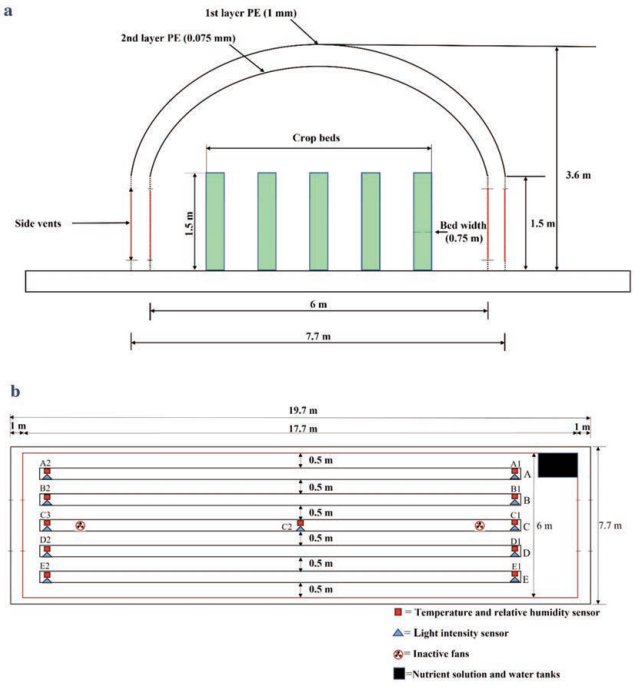

Figure 1. Schematic view of the experimental greenhouse: overall layout (**a**) and cross-section showing the position of sensors, fans, and nutrient/water tanks (**b**).

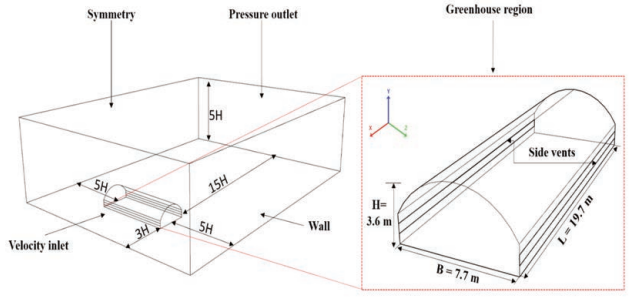

Figure 2. 3D computational domain of the experimental greenhouse: configuration including geometry and dimensions.

Model validation

The accuracy of the numerical model in predicting the internal thermal environment was assessed by comparing simulated temperature values with experimental measurements. To quantify the agreements, we employed two standard statistical measures: the root mean square error (RMSE) and the mean absolute error (MAE).

The RMSE serves as an indicator of the model's sensitivity and its ability to capture extreme values. On the other hand, the MAE provides insight into the model's overall accuracy. Both metrics are interpreted on a "smaller is better" basis, that is, lower values of RMSE and MAE indicate higher model accuracy.

These error measures can be mathematically represented as follows:

$$MAE = \frac{\sum_{i-1}^{n} (P_i - O_i)}{n} \quad \text{(Eq. 4)}$$

$$RMSE = \sqrt{\frac{\sum_{i-1}^{n} (P_i - O_i)^2}{n}} \quad \text{(Eq. 5)}$$

where P_i is the measured value, O_i is the simulated value, and n is the number of measured values.

Results and Discussion

Daily environmental variation

Environmental conditions inside and outside the greenhouse environment are critical factors that influence crop performance in naturally ventilated environments. These conditions affect processes such as photosynthetic electron transport, carbon assimilation, susceptibility to pests and diseases, and overall quality of plant growth and development (Li *et al*., 2023). Consequently, this study examines the environmental variability inside and outside the greenhouse during the experimental period.

Figures 4 and 5 show the average hourly daily environmental conditions (indoor temperature, relative humidity, outdoor solar radiation, and wind speed) on (a) June 1 a typical sunny day, and (b) June 20, a typical cloudy day.

On June 1, the mean temperature inside the greenhouse was 29.3°C (±11.7 °C), influenced by outdoor weather conditions, particularly at sunrise and sunset when solar radiation most impacts the thermal environment. The outdoor mean temperature was 20.7°C (±4.6 °C). Solar radiation inside the greenhouse had a mean value of 785 W/m² (±851 W/m²), and the maximum indoor temperature was 48.4°C at 11:00. Between 0:00 and 6:00, the indoor and outdoor temperatures were similar, indicating balanced heat transfer, with convective heat transfer dominant. From 6:00 onward, as the sun rose, solar radiation increased, leading to a larger indoor-outdoor temperature difference, which gradually decreased after peak afternoon hours.

On June 20, indoor temperature and solar radiation were lower compared to June 1, with mean values of 24.6°C (±3.3°C) and 156 W/m² (±180 W/m²), respectively. The maximum nighttime temperature inside the greenhouse was 30.4°C at 13:00. Between 0:00 and 6:00, indoor and outdoor temperatures remained close, reflecting balanced heat transfer, though the overall temperature difference was smaller than on June 1 due to overcast conditions.

The mean indoor relative humidity on June 1 was 53 % (±29%), with outdoor RH at 66 % (±21%). Daytime differences were larger than nighttime due to higher outdoor temperatures reducing RH, while warmer air entering through side vents lowered indoor RH further. At night, cooler outdoor air and reduced air exchange caused indoor and outdoor RH to converge.

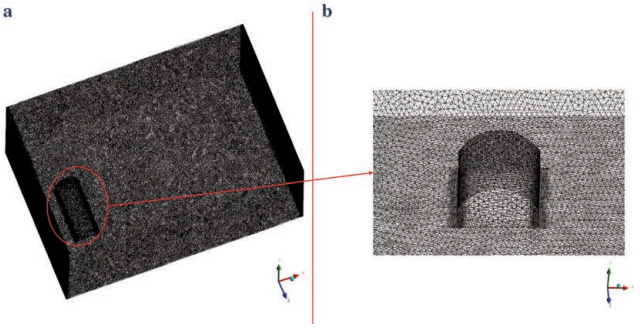

Figure 3. Mesh structure of the experimental greenhouse: experimental greenhouse within computational domain (**a**) and greenhouse structure (**b**).

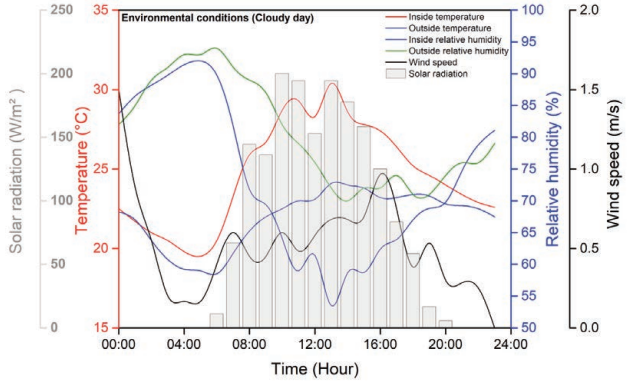

Figure 4. Environmental conditions on a typical sunny day.

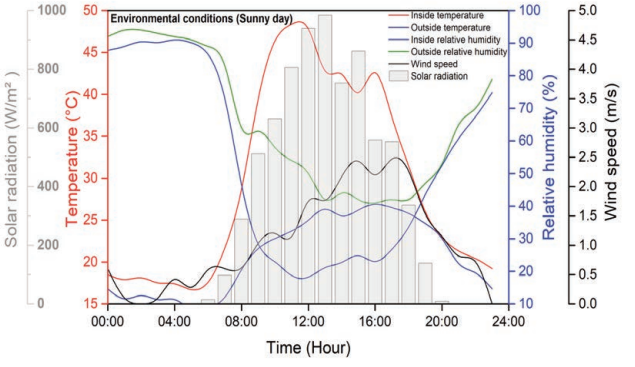

Figure 5. Environmental conditions on a typical cloudy day.

On June 20, indoor RH was higher than on June 1, with a mean of 74% (±12%), and outdoor RH was 81% (±8%), reflecting more stable conditions. The daytime difference between indoor and outdoor RH was larger than at night, contrasting with June 1. Lower solar radiation and cooler outdoor temperatures reduced evaporative demand, keeping indoor RH higher than outdoor.

Outside wind speeds on June 1 ranged from 0 m/s at night to a maximum of 2.6 m/s at 15:00 and 17:00, with a mean of 1.1 m/s (±0.9 m/s). On June 20, wind speeds were lower, from 0 m/s at night to 1.5 m/s, with a mean of 0.5 m/s (±0.4 m/s), reflecting more stable atmospheric conditions.

Solar radiation outside the greenhouse on June 1 ranged from 0 W/m² at night to a maximum of 983 W/m² at 13:00, with a mean of 312 W/m² (±360 W/m²). On June 20, it ranged from 0 W/m² at night to a maximum of 200 W/m² at 10:00, with a mean of 72 W/m² (±79 W/m²), reflecting diffuse radiation under cloud cover.

Correlation analysis

To thoroughly examine the relationship between each indoor and outdoor climatic variable measured, a correlation heatmap of all variables on the two days (Figures 6 and 7) was conducted. On June 1, there was a strong correlation among environmental parameters as a result of solar radiation and temperature fluctuations. Indoor temperature showed a high positive correlation with outdoor temperature (r=0.84) and solar radiation (r=0.96), which suggested that greenhouse thermal conditions were strongly influenced by external solar input. Conversely, indoor temperature had a strong negative correlation with indoor relative humidity (r= -0.95) and outdoor relative humidity (r= -0.80), a common phenomenon where increased temperature leads to reduced relative humidity due to increased evaporative demand (Li *et al*., 2023; Mao *et al*., 2024). Indoor solar radiation showed a positive correlation with indoor temperature (r=0.88) and outdoor solar radiation (r=0.85), which reinforced the occurrence that energy penetration into the greenhouse followed external solar radiation patterns. However, indoor relative humidity correlated negatively with both indoor (r= -0.84) and outdoor solar radiation (r= -0.68), as higher energy levels promoted increased transpiration, reducing humidity. Outdoor wind speed had a notable positive correlation with outdoor temperature (r=0.90) but showed a moderate correlation with indoor temperature (r=0.72), which indicated its effect in heat exchange and convective cooling.

On June 20, under cloudy conditions, the correlations showed weaker dependencies among certain variables, which reflected the dampening effect of cloud cover on temperature fluctuations and solar radiation. Indoor temperature retained a strong negative correlation with indoor relative humidity (r= -0.97) but showed a lower correlation with outdoor temperature (r=0.80) compared to the sunny day, which indicated reduced external influence due to lower solar radiation. Similarly, the correlation between indoor temperature and outdoor solar radiation decreased to r=0.92, compared to 0.96 on the sunny day, which further emphasized the buffering effect of cloud cover. Indoor solar radiation remained positively correlated with outdoor solar radiation (r=0.95) but had a weaker correlation with indoor temperature (r=0.86), showing that while energy levels were still influenced by external conditions, their effect on greenhouse thermal conditions was diminished. Notably, the correlation between wind speed and other variables weakened significantly; for example, wind speed and outdoor temperature had a correlation of only r=0.36, compared to 0.90 on the sunny day. This suggested that external air movement

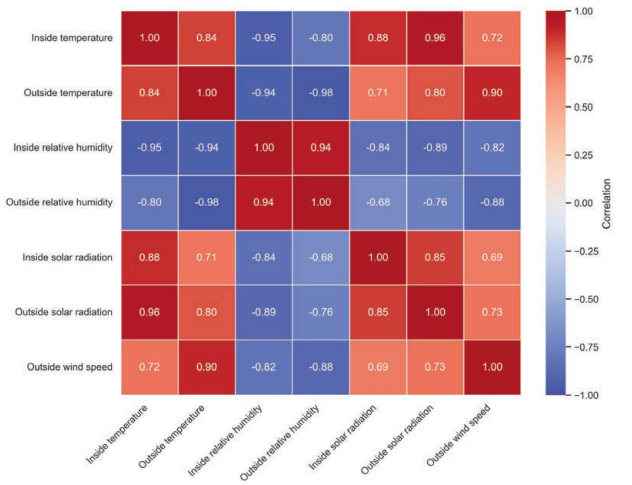

Figure 6. Correlation heatmap between variables on sunny day.

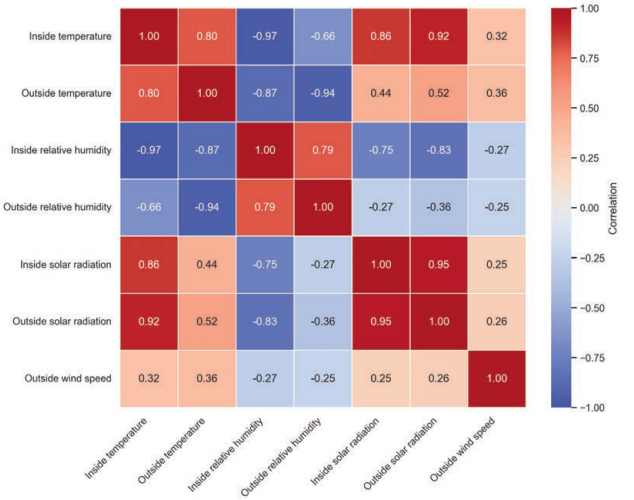

Figure 7. Correlation heatmap between variables on cloudy day.

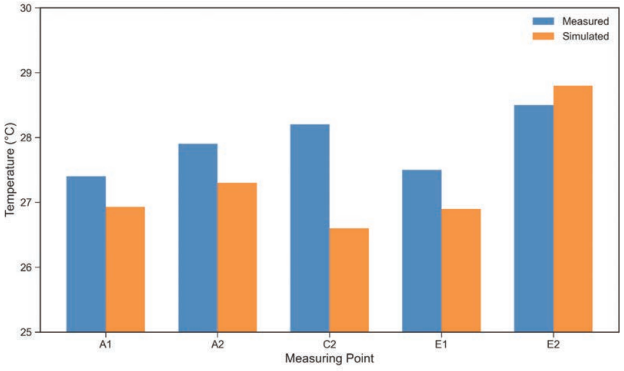

Figure 8. Comparison of simulated and experimental temperature values.

had a reduced impact on greenhouse thermal dynamics under stable, cloudy conditions.

Overall, it could be deduced that on sunny days, greenhouse environmental conditions are heavily influenced by external solar radiation, resulting in strong correlations among temperature, humidity, and energy levels. However, on cloudy days, the greenhouse environment exhibits more stability, with lower correlations between external and internal variables. These findings further emphasize the necessity of considering the dynamic interactions of indoor and outdoor variables in the CFD model.

Model validation

The average simulated temperature measured at points A1, A2, C2, E1, and E2 (Figure 1b) at 12:00 on June 20 was used to validate the model. Upon extraction of the results from the simulation and comparison against actual values, it was observed that the simulated values and measured values were consistent and in good agreement. Figure 8 shows the comparison between the measured and simulated temperatures in the greenhouse. The RMSE and MAE values for temperature were 0.847°C and 0.714°C, respectively. The differences between the measured and simulated temperatures in the study were deemed acceptable, indicating that the developed greenhouse CFD model is effective and suitable for further analysis of the greenhouse environment distribution. Although the model was validated against measured temperatures at points A1, A2, C2, E1, and E2 with good agreement, additional spatial and temporal measurements on more days using more data could further check and improve the model's accuracy and robustness in future work.

Spatial distribution of air temperature

The validated CFD model was used to examine the differences in the internal microclimate during the highest thermal stress, recorded on June 1 at 11:00. To give a clear three-dimensional view of the environmental patterns, the analysis focused on the distribution of air temperature across selected cross-sections. A total of eight virtual planes were defined within the greenhouse for this purpose. Four transverse planes (in the YZ orientation) were created at equal intervals along the greenhouse's 19.7 m length, positioned at X = 3.94 m, 7.88 m, 11.82 m, and 15.76 m. These planes were selected to capture the change in the temperature as air moves from the windward to the leeward side, revealing vertical layers and side-to-side differences. Similarly, four longitudinal planes (in the XY orientation) were established at equal intervals across the greenhouse's 7.7 m width, located at Z = 1.54 m, 3.08 m, 4.62 m, and 6.16 m. This arrangement was selected to study the airflow and temperature distribution along the main ventilation route, showing the gradients from the inlet to the outlet vent. While the simulation did not include specific crop models, these planes were placed to reflect conditions typical to a crop canopy area, offering important insights into the consistency of the growing environment. This selection also allows a more detailed evaluation of the ventilation performance and the degree of thermal uniformity across the main cultivation zones.

Figures 9 and 10 illustrate the air temperature distribution across transverse (YZ) and longitudinal (XY) planes. The air temperature varied significantly, from a minimum of approximately 296 K near the inlet vent to a maximum of 321 K in the upper regions. The transverse planes showed vertical thermal stratification common to greenhouses, as reported in Saberian and Sajadiye (2019) and Bazgaou *et al*. (2023). This temperature gradient can be explained by the difference in density between warm and cold air as solar radiation heats the floor, causing this hot, less dense air to rise and accumulate in the upper dome, while cooler air remains trapped in the lower part. This buoyancy-driven effect, often referred to as the "stack effect," is a main driver of natural ventilation. The relatively lower temperature observed near the windward vent in Figure 9 is due to the intrusion of cooler ambient air, a direct result of the ventilation process. In addition, the observed vertical gradient of roughly 10-15 K between the lower and upper regions indicates limited vertical mixing. This strong gradient suggests that the existing vent configuration does not sufficiently remove accumulated heat from the upper layer.

The longitudinal planes in Figure 10 provide a top-down view of the horizontal thermal heterogeneity and the progression of air as it moves through the greenhouse structure. The area near the windward vent consistently showed the lowest temperatures (indicated by blue contours, ~310 K), confirming the path of the incoming cool air jet. As this air traverses the length of the greenhouse, it is progressively heated by absorbing convective heat from the floor and mixing with the warmer internal air, leading to the highest temperatures being concentrated on the leeward side. Furthermore, the longitudinal plane closest to the roof displayed the most extreme conditions, with a large region of hot air (>320 K) in the leeward corner. This consistent rise in temperature along the longitudinal direction (with an approximate increase of 8–12 K from inlet to outlet) highlights a gradual loss of inlet jet momentum, causing the cool airflow to remain confined to the lower canopy level. From both planes, a comprehensive three-dimensional pattern was observed. A jet of cool air enters from the windward side vent, primarily affecting the lower level. This air warms as it travels the length of the greenhouse, while simultaneously, hot air heated by the floor rises and is pushed towards the leeward side.

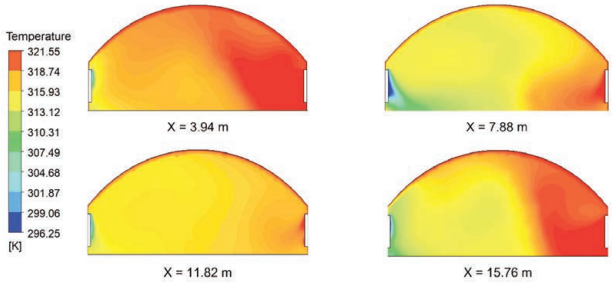

Figure 9. Simulated temperature distribution on the four tranverse (YZ) planes across the length of the greenhouse.

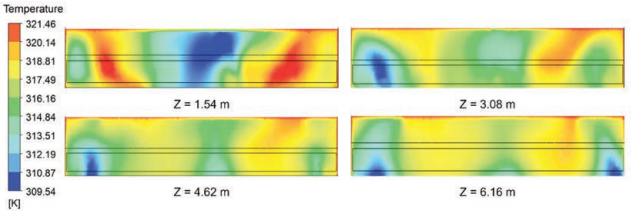

Figure 10. Simulated temperature distribution on the four longitudinal (XY) planes across the length of the greenhouse.

This results in the accumulation of the hottest air in the upper, leeward corner of the structure, showing a significant non-uniformity in the thermal environment created by the natural ventilation system under high solar load. This spatial heterogeneity is a challenge in naturally ventilated greenhouses and can significantly impact crop uniformity and yield. This behavior indicates that the current natural ventilation strategy is insufficient for extracting buoyant heat from the upper zones, leading to reduced ventilation effectiveness under peak radiation conditions. The strong spatial heterogeneity observed here may cause substantial differences in crop temperature exposure along the greenhouse, potentially affecting growth uniformity and yield. Overall, these results confirm that the greenhouse experiences strong stratification, limited vertical mixing, and asymmetric ventilation efficiency, conditions that justify future optimization of vent size, placement, and airflow pathways.

Conclusions

This study employed a 3D CFD model to analyze and predict the temperature distribution within a naturally ventilated single-span greenhouse, providing a detailed understanding of its thermal performance under high solar load. The model's predictions showed good agreement with experimental measurements (RMSE=0.847°C), confirming its reliability for microclimate analysis. The investigation revealed that the internal thermal environment is highly heterogeneous, with an overall temperature difference of up to 25°C observed within the structure. This non-uniformity is characterized by strong vertical stratification driven by the buoyancy of solar-heated air (the "stack effect") and a distinct longitudinal gradient, which results in the accumulation of the hottest air in the upper leeward regions of the greenhouse. This finding confirms that relying on natural ventilation alone presents a significant challenge to maintaining consistent growing conditions. The practical implications of these findings are important for improving greenhouse design and management. The detailed thermal maps identifying a persistent "hot spot" in the upper leeward corner offer actionable insights, suggesting that sensor placement, vent configurations, or the location of heat-sensitive crops should be reconsidered. The demonstrated limitation of side vents in achieving vertical mixing provides a strong justification for exploring supplementary systems, such as horizontal airflow fans or roof vents, to create a more uniform environment. The validated model itself serves as a valuable and cost-effective tool for testing such design modifications virtually before implementation.

Future research should build upon this foundation to enhance the model's predictive capabilities. Key recommendations include incorporating a crop sub-model to account for the aerodynamic and transpiration effects of a mature plant canopy, as well as the thermal influence of internal structures like benches. Expanding the study to include transient simulations would also offer deeper insights into the diurnal heating and cooling cycles. Ultimately, this research contributes to the development of more resilient protected agriculture systems by providing a detailed understanding of the thermal dynamics that govern them.

References

Aguilar-Rodríguez CE, Flores-Velázquez J, Rojano F, Flores-Magdaleno H, Panta ER, 2021. Simulation of water vapor and near infrared radiation to predict vapor pressure deficit in a greenhouse using CFD. Processes 9:1587.

Akpenpuun TD, Ogunlowo QO, Na WH, Rabiu A, Adesanya MA, Dutta P, et al. 2023a. Review of temperature management strategies and techniques in the greenhouse microenvironment. Adeleke Uni J Engin Technol 6:126-147.

Akpenpuun TD, Ogunlowo QO, Na WH, Rabiu A, Adesanya MA, Kim HT, Lee HW, 2023b. Maximising strawberry yield in single-layered and double-layered gothic greenhouses: a microclimate approach. J Appl Sci Environ Manag 27:1371-1377.

Akrami M, Javadi AA, Hassanein MJ, Farmani R, Dibaj M, Tabor GR, Negm A, 2020a. Study of the effects of vent configuration on mono-span greenhouse ventilation using computational fluid dynamics. Sustainability 12:986.

Akrami M, Salah AH, Javadi AA, Fath HES, Hassanein MJ, Farmani R, et al., 2020b. Towards a sustainable greenhouse: Review of trends and emerging practices in analysing greenhouse ventilation requirements to sustain maximum agricultural yield. Sustainability 12:2794.

Amara HB, Bouadila S, Fatnassi H, Arici M, Guizani AA, 2021. Climate assessment of greenhouse equipped with south-oriented PV roofs: An experimental and computational fluid dynamics study. Sustain Energy Technol Assess 45:101100.

Ayuga F, 2015. Present and future of the numerical methods in buildings and infrastructures areas of biosystems engineering. J Agric Eng 46:436.

Bazgaou A, Fatnassi H, Bouharroud R, Tiskatine R, Wifaya A, Demrati H, et al., 2023. CFD modeling of the microclimate in a greenhouse using a rock bed thermal storage heating system. Horticulturae 9:183.

Benni S, Tassinari P, Bonora F, Barbaresi A, Torreggiani D, 2016. Efficacy of greenhouse natural ventilation: Environmental monitoring and CFD simulations of a study case. Energy Build 125:276-286.

Blanco I, Luvisi A, De Bellis L, Schettini E, Vox G, Scarascia Mugnozza G, 2022. Research trends on greenhouse engineering using a science mapping approach. Horticulturae 8:833.

Choab N, Allouhi A, El Maakoul A, Kousksou T, Saadeddine S, Jamil A, 2019. Review on greenhouse microclimate and application: Design parameters, thermal modeling and simulation, climate controlling technologies. Solar Energy 191:109-137.

Chu CR, Lan TW, Tasi RK, Wu TR, Yang CK, 2017. Wind-driven natural ventilation of greenhouses with vegetation. Biosyst Eng 164:221-234.

Elanchezhian A, Basak JK, Park J, Khan F, Okyere FG, Lee Y, et al., 2020. Evaluating different models used for predicting the indoor microclimatic parameters of a greenhouse. Appl Ecol Environ Res 18:2141-2161.

Ghani S, El-Bialy EMAA, Bakochristou F, Mohamed Rashwan M, Mohamed Abdelhalim A, Mohammad Ismail S, Ben P, 2020. Experimental and numerical investigation of the thermal performance of evaporative cooled greenhouses in hot and arid climates. Sci Technol Built Environ 26:141-160.

Gołasa P, Wysokiński M, Bieńkowska-Gołasa W, Gradziuk P, Golonko M, Gradziuk B, et al., 2021. Sources of greenhouse gas emissions in agriculture, with particular emphasis on emissions from energy used. Energies 14:3784.

Hou Y, Li A, Li Y, Jin D, Tian Y, Zhang D, et al., 2021. Analysis of microclimate characteristics in solar greenhouses under natural ventilation. Build Simul 14:1811-1821.

Khudoyberdiev A, Ullah I, Kim D, 2021. Optimization-assisted water supplement mechanism with energy efficiency in IoT based greenhouse. J Intell Fuzzy Syst 40:10163-10182.

Kim R, Hong S, Lee I, Kwon K. 2017. Evaluation of wind pressure acting on multi-span greenhouses using CFD technique, Part 2: Application of the CFD model. Biosyst Eng 164:257-280.

Korean Meteorological Administration [Internet], n.d. [Climate characteristics by region in Korea].[Website in Korean]. Accessed on: 22 March 2025. Available from: https://www.weather.go.kr/w/climate/statistics/regional-char.do?area=7

Lamichhane P, Adhikari J, Poudel A, 2023. Protected cultivation of horticultural crops in Nepal: Current practices and future needs. Arch Agric Environ Sci 8:268-273.

Lawrence J, Simpson L, Piggott A, 2017. Protected agriculture: a climate change adaptation for food and nutrition security. In: Information Resources Management Association (ed.), Natural resources management: concepts, methodologies, tools, and applications. New York, IGI Global; pp. 140-158.

Lee S, Lee I, Kim R, 2018. Evaluation of wind-driven natural ventilation of single-span greenhouses built on reclaimed coastal land. Biosyst Eng 171:120-142.

Li H, Li A, Hou Y, Zhang C, Guo J, Li J, et al., 2023. Analysis of heat and humidity in single-slope greenhouses with natural ventilation. Buildings 13:606.

Li W, Zhuang M, Feng L, Wei W, Xia L, Yang Y, 2025. Carbon and reactive nitrogen footprint of greenhouse versus open-field vegetable production in China. Resour Conserv Recycl 221:108400.

Li Y, Sun F, Shi W, Liu X, Li T, 2022. Numerical simulation of ventilation performance in mushroom solar greenhouse design. Energies 15:5899.

Mao Q, Li H, Ji C, Peng Y, Li T, 2024. Experimental study of ambient temperature and humidity distribution in large multi-span greenhouse based on different crop heights and ventilation conditions. Appl Therm Eng 248:123176.

Nebbali R, Roy JC, Boulard T, Makhlouf S, 2006. Comparison of the accuracy of different CFD turbulence models for the prediction of the climatic parameters in a tunnel greenhouse. Acta Hortic 719:287-294.

Revathi S, Sivakumaran N, Radhakrishnan TK, 2021. Design of solar-powered forced ventilation system and energy-efficient thermal comfort operation of greenhouse. Mater Today Proc 46:9893-9900.

Saberian A, Sajadiye SM, 2019. The effect of dynamic solar heat load on the greenhouse microclimate using CFD simulation. Renew Energy 138:722-737.

Santolini E, Pulvirenti B, Benni S, Barbaresi L, Torreggiani D, Tassinari P, 2018. Numerical study of wind-driven natural ventilation in a greenhouse with screens. Comput Electron Agric 149:41-53.

Senhaji A, Mouqallid M, Majdoubi H, 2019. CFD assisted study of multi-chapels greenhouse vents openings effect on inside airflow circulation and microclimate patterns. Open J Fluid Dynam 9:119-139.

Villagran E, Bojacá C, Akrami M, 2021. Contribution to the sustainability of agricultural production in greenhouses built on slope soils: A numerical study of the microclimatic behavior of a typical Colombian structure. Sustainability 13:4748.

Villagrán EA, Baeza Romero EJ, Bojacá CR, 2019. Transient CFD analysis of the natural ventilation of three types of greenhouses used for agricultural production in a tropical mountain climate. Biosyst Eng 188:288-304.

Yeo UH, Lee SY, Park SJ, Kim JG, Choi YB, Kim RW, et al., 2022. Rooftop greenhouse: (1) design and validation of a BES model for a plastic-covered greenhouse considering the tomato crop model and natural ventilation characteristics. Agriculture 12:903.

Yin H, Wang K, Zeng J, Pang Z, 2024. CFD analysis and optimization of a plastic greenhouse with a semi-open roof in a tropical area. Agronomy 14:876.

Zhang G, Fu Z, Yang M, Liu X, Dong Y, Li X, 2019. Nonlinear simulation for coupling modeling of air humidity and vent opening in Chinese solar greenhouse based on CFD. Comput Electron Agric 162:337-347.

Zhang L, Liu X, Shi W, Li T, Ji J, 2022. Study of a novel front-roof-back natural ventilation system for Chinese solar greenhouses. R Soc Open Sci 9:220251.

Online Supplementary Material

Equations of airflow pattern

Received: 12 February 2025; Accepted: 21 January 2026.

Contributions: Oluwasegun Moses Ogundele, conceptualization, methodology, formal analysis, writing-original draft, investigation, data curation, software. Sijan Karki, Niraj Tamrakar, investigation, resources, writing-review & editing. Jung-Hoo Kook, Jeong-In Choi, data curation, validation. Sang-Min Kim, Timothy Denen Akpenpuun, investigation, software. Reginald Gbenga Azuatalam, investigation, resources, writing-review & editing. Hyeon Tae Kim, resources, supervision, project administration, funding acquisition, writing-review & editing. All the authors read and approved the final version of the manuscript and agreed to be accountable for all aspects of the work.

Conflict of interest: the authors declare conflicts of interest and all authors confirm accuracy.

Availability of data and material: the data used to support the findings of this study are available from the corresponding author upon request.

Funding: this work was funded and supported by the Glocal University 30 Project Fund of Gyeongsang National University in 2025.